Contribution from the Department of Physics, The Pennsylvania State University, University Park, Pennsylvania 16802, and Department of Chemistry, University of Southern California, Los Angeles, California 90089-1062

Susceptibility and Mössbauer Analysis of a High-Spin Ferrous Synthetic Heme with Unusually Large Quadrupole Splitting

Ben A. Shaevitz,[†] George Lang,*[,†] and Christopher A. Reed*[,‡]

Received June 7, 1988

Magnetic susceptibility and Mössbauer spectroscopy have been used to probe the five-coordinate anionic ferrous heme [Fe(TPP)(OPh)]$^-$ as its polycrystalline salt [Na(dibenzo-18-crown-6)(THF)$_2$][Fe(TPP)(OPh)] (TPP = tetraphenylporphyrinate, OPh = phenoxide). This species is a synthetic model for the P-460 center of hydroxylamine oxidoreductase from *Nitrosomonas europeae*. The magnetic susceptibility was recorded at fields of 0.1 and 1.0 T in the temperature range 2–300 K. The high-temperature effective Bohr magneton number of 5.1 is consistent with a high-spin ferrous ion. The susceptibility data were analyzed by a $S = 2$ spin Hamiltonian with weak antiferromagnetic exchange between pairs of neighboring iron atoms. The fits gave $D = -1.6$ cm^{-1}, $E = 0$, $J = -0.08$ cm^{-1}, and $g = 2$ in excellent agreement with the Mössbauer results. Mössbauer spectra were recorded at selected temperatures from 4.2 to 195 K and applied magnetic fields of 0–6 T. The zero-field results of $\delta = 1.032$ mm/s and $\Delta E_q = 4.008$ mm/s at 4.2 K are consistent with a five-coordinate high-spin ferrous ion, and the small temperature dependence of the quadrupole splitting suggests a well-isolated ground state. High-field Mössbauer data were analyzed by using the phenomenological model of the internal magnetic field $\vec{H}_{int} = \tilde{\omega}\cdot\vec{H}_{app}$ and also by the coupled $S = 2$ spin Hamiltonian. The $T \geq 16$ K data were well simulated by the phenomenological model with an axial $\tilde{\omega}$ aligned with an axial electric field gradient (EFG), with $V_{zz} > 0$ and $\omega_z/\omega_\perp = 0.7 \pm 0.1$. The independent spin-Hamiltonian treatment yielded an axial splitting with electronic parameters $D = -1.60$ cm^{-1}, $E = 0$, $J = -0.08$ cm^{-1}, and $g = 2$ in a frame aligned with the axial EFG. These fits also yielded $V_{zz} > 0$ and the magnetic hyperfine tensor $\tilde{A}^*/g_n^*\beta_n = (-17.6, -17.6, -12.8)$ T/unit spin also aligned with the EFG. Both the high-temperature $\omega_z/\omega_\perp$ ratio and the sign of the EFG suggest that the sixth 3d electron is in an oblate orbital, $|xy\rangle$. This identifies the ground state as $^5A_2$ in C_{2v} symmetry (or $^5B_2$ in C_{4v} symmetry).

Introduction

Attention has recently been drawn to the unusually large quadrupole splittings seen in a new type of hemoprotein unique to ammonia-oxidizing bacteria[1] and in a number of ferrous porphyrin complexes.[2-5] Hydroxylamine oxidoreductase from *Nitrosomonas europeae* is a large multi-heme enzyme containing several *c*-type hemes along with an unusual prosthetic group termed P-460.[1,6] Although its precise chemical nature is unknown, spectral evidence suggests that in its reduced state P-460 is a five-coordinate high-spin ferrous heme-like moiety. Its quadrupole splitting of 4.21 mm/s at 4.2 K is very much larger than anything previously observed and characterizes the active site as something quite distinct from hemoglobin or cytochrome P-450. The first synthetic porphyrin to show a comparably large quadrupole splitting was the fortuitously prepared chloro-ligated heme [Fe(PF)(Cl)]$^-$ (PF = picket-fence porphyrin).[2] Subsequent studies by Silver[3,4] and by Weiss and Trautwein[5] suggest that large quadrupole splittings are a distinctive feature of high-spin ferrous porphyrins of the general formula [Fe(Porph)(X)]$^-$, where X is an anionic oxygen donor (OH^-, RO^-, $RCOO^-$) or halide. X-ray structural data are now available for a number of such picket-fence porphyrin derivatives.[2,5]

To date, Mössbauer studies on the synthetic hemes have been restricted to zero applied fields. There is, however, a great deal of electronic information in the paramagnetic behavior. In previous work we have shown how field- and temperature-dependent Mössbauer spectroscopy can be used to probe the nature of high-spin ferrous porphyrin complexes that are closely related to deoxyhemoglobin.[7,8] More recently, we have shown that this approach becomes more powerful when combined with a simultaneous study of low-temperature magnetic susceptibility.[9-13] This complementary approach is taken in the present work and proves to be particularly useful for the parameterization of key electronic features of [Fe(TPP)(OPh)]$^-$, a new member of the class of ferrous hemes with large quadrupole splitting.[14] The data have been analyzed in terms of a phenomenological model of the internal magnetic field and also by a $S = 2$ spin Hamiltonian as first steps toward a deeper theoretical interpretation.

Experimental Section

Sample Preparation. All manipulations were carried out in a Vacuum Atmospheres Corp. inert-atmosphere glovebox (O_2, H_2O < 1 ppm). Fe(TPP)(THF)$_2$ (0.165 g),[15] sodium phenoxide (0.08 g), and dibenzo-18-crown-6 (0.06 g) from Aldrich Chemical Co. were heated in 40 mL of tetrahydrofuran (THF) for about 3 min. The bright green solution was filtered through a fine frit and left overnight to crystallize. The resulting sparkling purple plates were collected by filtration, washed with THF, and allowed to dry (0.213 g, 81%). Anal. Calcd for [Na(dibenzo-18-crown-6)(THF)$_2$][Fe(TPP)(OPh)], $C_{78}H_{73}NaFeN_4O_9$: C, 72.66; H, 5.71; N, 4.34. Found: C, 72.70; H, 6.01; N, 4.23.

Samples for susceptibility measurement were finely ground and packed tightly into preweighed and precalibrated aluminum buckets. A typical sample size was 35 mg. Mössbauer samples (~100 mg) were lightly ground and immobilized by solidifying into melted paraffin wax within a 1 cm diameter Lucite dish.

Magnetic Susceptibility Measurements. Susceptibility measurements were made on a SHE Corp. SQUID susceptometer, Model 905. Field calibration was checked at both 0.1 and 1.0 T with a chemical standard of known Curie law behavior. Reproducibility of data within 2% was usually found, although it was often better. A diamagnetic correction of -1073×10^{-6} cgsμ was applied by using the measured value of -700×10^{-6} cgsμ for TPP[16] and Pascal's constants[17] for the remaining atoms.

[†] The Pennsylvania State University.
[‡] University of Southern California.

(1) Andersson, K. K.; Kent, T. A.; Lipscomb, J. D.; Hooper, A. B.; Munck, E. *J. Biol. Chem.* **1984**, *259*, 6833.
(2) Schappacher, M.; Ricard, L.; Weiss, R.; Montiel-Montoya, R.; Gonser, U.; Bill, E.; Trautwein, A. *Inorg. Chim. Acta* **1983**, *78*, L9.
(3) Silver, J.; Luckas, B. *Inorg. Chim. Acta* **1983**, *80*, 107.
(4) Silver, J.; Lukas, B.; Al-Jaff, G. *Inorg. Chim. Acta* **1984**, *91*, 125.
(5) Narsi, H.; Fischer, J.; Weiss, R.; Bill, E.; Trautwein, A. *J. Am. Chem. Soc.* **1987**, *109*, 2549.
(6) Prince, R. C.; Hooper, A. B. *Biochemistry* **1987**, *26*, 970.
(7) Kent, T. A.; Spartalian, K.; Lang, G.; Yonetani, T.; Reed, C. A.; Collman, J. P. *Biochim. Biophys. Acta* **1979**, *580*, 245.
(8) Boso, B.; Lang, G.; Reed, C. A. *J. Chem. Phys.* **1983**, *78*, 2561.
(9) Lang, G.; Boso, B.; Erler, B. S.; Reed, C. A. *J. Chem. Phys.* **1986**, *84*, 2998.
(10) Gupta, G. P.; Lang, G.; Scheidt, W. R.; Geiger, D. K.; Reed, C. A. *J. Chem. Phys.* **1985**, *83*, 5945.
(11) Gupta, G. P.; Lang, G.; Scheidt, W. R.; Geiger, D. K.; Reed, C. A. *J. Chem. Phys.* **1986**, *85*, 5212.
(12) Gupta, G. P.; Lang, G.; Reed, C. A.; Shelly, K.; Scheidt, W. R. *J. Chem. Phys.* **1987**, *86*, 5288.
(13) Gupta, G. P.; Lang, G.; Lee, Y. J.; Scheidt, W. R.; Shelly, K.; Reed, C. A. *Inorg. Chem.* **1987**, *26*, 3022.
(14) Shaevitz, B. A.; Lang, G.; Reed, C. A. *Bull. Am. Phys. Soc.* **1987**, *32*, 411.
(15) Reed, C. A.; Mashiko, T.; Scheidt, W. R.; Spartalian, K.; Lang, G. *J. Am. Chem. Soc.* **1980**, *102*, 2302.
(16) Eaton, S. S.; Eaton, G. R. *Inorg. Chem.* **1980**, *19*, 1095.
(17) Boudreaux, E. A.; Mulay, L. N. *Applications of Molecular Paramagnetism*; Wiley: New York, 1976.

0020-1669/88/1327-4607$01.50/0

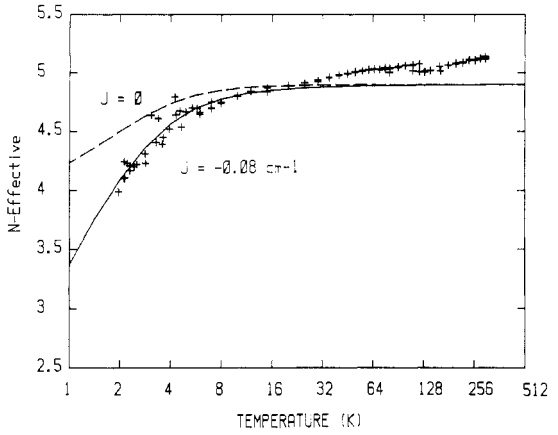

Figure 1. Effective Bohr magneton number for $[Fe(TPP)(OPh)]^-$ as a function of temperature, where $N_{eff} = [3kT\chi/\beta^2]^{1/2}$ and χ is the susceptibility per heme unit. The solid line is a calculation based on the Hamiltonian of eq 1 and 2 with the parameters $D = -1.6$ cm^{-1}, $E = 0$, $J = -0.08$ cm^{-1}, and $g = 2$. The dashed line is a calculation made with the same parameters as above except that $J = 0$. The crosses are measurements made in an applied magnetic field of 0.1 T.

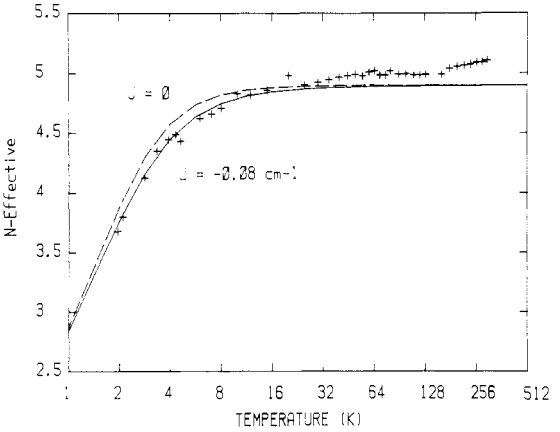

Figure 2. Effective Bohr magneton number for $[Fe(TPP)(OPh)]^-$ as a function of temperature. The solid line is a calculation based on the Hamiltonian of eq 1 and 2 with the parameters $D = -1.6$ cm^{-1}, $E = 0$, $J = -0.08$ cm^{-1}, and $g = 2$. The dashed line is a calculation made with the same parameters as above except that $J = 0$. The crosses are measurements made in an applied magnetic field of 1.0 T.

Mössbauer Measurements. Mössbauer spectra were recorded in horizontal transmission geometry by using a constant-acceleration spectrometer operated in connection with a 256-channel analyzer in the time scale mode. The source of γ radiation consisted of approximately 50 mCi of ^{57}Co diffused in rhodium foil. The source was kept at room temperature for all experiments. The spectrometer was calibrated with a metallic iron foil, and zero velocity was taken as the centroid of its room-temperature Mössbauer spectrum. The calibrations yielded a typical line width of 0.25 mm/s (fwhm) and were stable to approximately 0.2% over the period of 1 week. The linearity of the velocity scale was better than 0.1%. High-field measurements were obtained using a split-coil superconducting magnet with the γ beam directed normal to the magnetic field. High-field runs typically took 36 h whereas 12 h was typical for a run in zero field. The sample temperature of 4.2 K was obtained by immersing the sample in liquid helium. Meaurements above 4.2 K were obtained by mounting the sample in a small counter-Dewar on a heated copper finger. The sample temperature was regulated by using an electronic controller with the heating element comprising one arm of a Wheatstone bridge.[18] The temperature was measured with an uncertainty of 3% by a gold–iron vs chromel thermocouple with the reference junction in good thermal contact with the liquid-helium bath.

Results

Magnetic Susceptibility. The magnetic susceptibility of $[Fe(TPP)(OPh)]^-$ was measured at 0.1 and 1.0 T in the temperature range 2–300 K. The effective number of Bohr magnetons, N_{eff}, has been plotted vs temperature in Figures 1 and 2. Figure 1 includes the results of three separate runs. We have chosen a logarithmic temperature scale in order to effectively display the rapid falloff of N_{eff} at low temperature, where zero-field splitting and weak inter-heme coupling become important. The room-temperature N_{eff} value is only a few percent higher than the spin-only value of 4.90. .The data in Figures 1 and 2 were analyzed by using the Hamiltonian

$$\mathcal{H} = \mathcal{H}_1(1) + \mathcal{H}_1(2) - J\vec{S}_1\cdot\vec{S}_2 \quad (1)$$

where

$$\mathcal{H}_1 = D[S_z^2 - S(S+1)/3] + E(S_x^2 - S_y^2) + g\beta\vec{H}_{app}\cdot\vec{S} \quad (2)$$

Here the first two terms of eq 1 represent the individual ions of an assumed dimer and the last term allows for an inter-heme exchange coupling. The meaning of the symbols in eq 2 are as follows: D and E describe the splittings in zero field, g is the electronic g factor, β is the Bohr magneton, H_{app} is the applied magnetic field, and $S_1 = S_2 = 2$. The Hamiltonian of eq 1 has been used extensively to treat coupling in five-coordinated ferric compounds.[9-13] The fits to the susceptibility data are shown as the solid lines in Figures 1 and 2 and assume the following values: $D = -1.6$ cm^{-1}, $E = 0$, $J = -0.08$ cm^{-1}, and $g = 2$. These values are a result of a simultaneous consideration of both the Mössbauer and susceptibility data. Neither Mössbauer nor susceptibility fits are improved by taking $E \neq 0$; large values of E are in fact ruled out by the susceptibility measurements. The sign of J indicates an antiferromagnetic interaction and results in a decrease of the low-temperature N_{eff} compared with that for the uncoupled case. Although it is possible to fit the susceptibility data without invoking inter-heme coupling, it requires $D = +3.2$ cm^{-1} and is impossible to reconcile with the Mössbauer data. We have been unsuccessful in obtaining single crystals suitable for X-ray structure determination, but our recent experience suggests dimeric association is very common with five-coordinate hemes. The anionic charge in the present compound is expected to diminish such associative tendencies, and this may explain why the strength of the coupling ($J = -0.08$ cm^{-1}) is 1 order of magnitude smaller than with the neutral species.[9-13]

We note that our calculated curves fall below the data in the high-temperature region, implying some unquenched orbital angular momentum. Preliminary calculations suggest that this deviation can be eliminated in a proper crystal field treatment. We defer a detailed discussion of this to a later paper, in which we hope to employ a spin-coupled crystal field calculation.

Zero-Field Mössbauer Spectra. Zero-field spectra of $[Fe(TPP)(OPh)]^-$ were recorded at eight temperatures between 4.2 and 195 K. At each temperature the spectrum consisted of a symmetric quadrupole-split doublet with an isomer shift $\delta \approx 1.0$ mm/s and a quadrupole splitting $\Delta E_q \approx 4.0$ mm/s. The isomer shift allows us unambiguously to classify the compound as a high-spin ferrous species, and the quadrupole splitting is among the largest recorded.[1-5,19-26] In order to determine the parameters

Table I. Mössbauer Parameters of $[Fe(TPP)(OPh)]^-$ at Various Temperatures in Zero Magnetic Field

T, K	δ, mm/s[a]	ΔE_q, mm/s[b]	Γ, mm/s
4.2	1.032	4.008	0.25
8.0	1.033	4.003	0.25
16.0	1.033	4.001	0.25
32.0	1.030	3.994	0.25
64.0	1.026	3.984	0.24
77.0	1.025	3.982	0.24
128.0	1.006	3.946	0.24
195.0	0.970	3.890	0.23

[a] With respect to metallic iron at room temperature. [b] $V_{zz} > 0$ and $\eta = 0$ at all temperatures.

(18) Window, B. *J. Sci. Instrum.* **1969**, *2*, 894 (Series 2).
(19) De Vries, J. L. K. F.; Keijzers, C. P.; De Boer, E. *Inorg. Chem.* **1972**, *11*, 1343.
(20) Konig, E.; Ritter, G.; Lindner, E.; Lorenz, I. P. *Chem. Phys. Lett.* **1972**, *13*, 70.

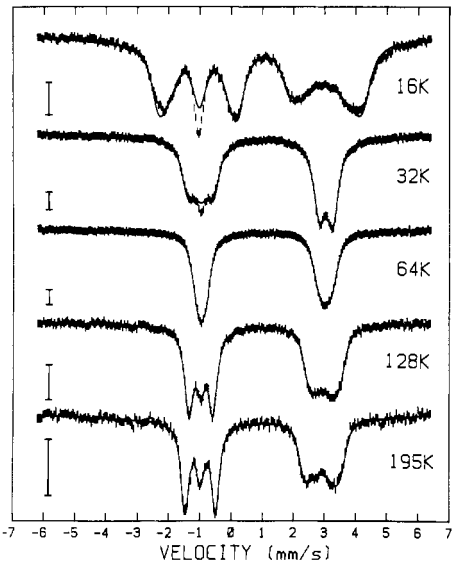

Figure 3. Mössbauer spectra of [Fe(TPP)(OPh)]⁻ in a transverse magnetic field of 6 T at the temperatures indicated. The solid lines are calculations based on the phenomenological model of eq 3 and 4 with parameters listed in Table II and plotted in Figure 5. Vertical bars indicate 1% absorption.

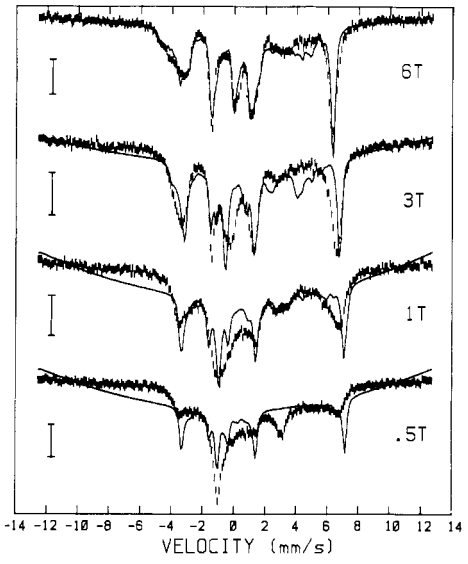

Figure 4. Mössbauer spectra of [Fe(TPP)(OPh)]⁻ at 4.2 K and in transverse magnetic fields as indicated. The solid lines are based on spin Hamiltonian method I, using eq 1, 2, 5, and 6 with parameters listed in Table III except for $\Delta = 0$. The curved base lines in the lower three simulations are artifacts of the fitting program, which in these poor-fit cases overestimates the counter solid angle effect. Vertical bars indicate 1% absorption.

δ, ΔE_q, and the Lorentzian line width Γ, a simplified version of the multiparameter least-squares fitting program of Lang and Dale[27] was used. The results are displayed in Table I. The uncertainty in these results is approximately ±0.005 mm/s. The variation of the isomer shift with temperature is consistent with that produced by a second-order Doppler shift. It is low as compared with those of most non-heme high-spin ferrous compounds, indicating a delocalization of the 3d electrons. The weak temperature dependence of the quadrupole splitting displayed in Table I reveals that the orbital ground state of the $(3d)^6$ electronic configuration is well isolated.

Table II. $\tilde{\omega}$-Tensor Parameters for Data in Figure 3[a]

T, K	$\omega_\perp$	ω_z	$\omega_z/\omega_\perp$	Γ, mm/s
16.0	−2.78	−2.36	0.85	0.50
32.0	−1.63	−1.20	0.74	0.43
64.0	−1.14	−0.63	0.56	0.38
128.0	−0.49	−0.34	0.69	0.34
195.0	−0.32	−0.24	0.75	0.29

[a] $V_{zz} > 0$ and $\eta = 0$ for all temperatures.

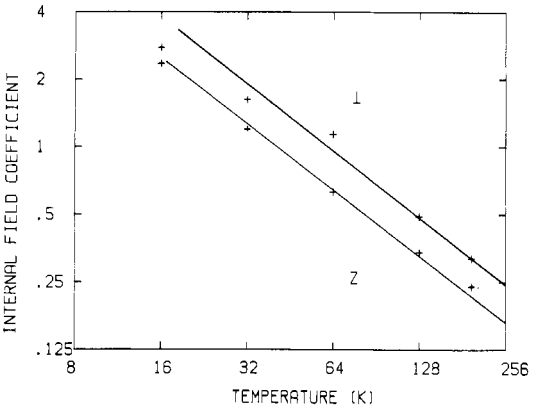

Figure 5. Internal field coefficients $\omega_\perp$ and ω_z as a function of temperature. The solid lines indicate a $1/T$ dependence.

High-Field Mössbauer Spectra. The Mössbauer spectra of [Fe(TPP)(OPh)]⁻ recorded at high magnetic field (0.5–6 T) and variable temperature (4.2–195 K) are displayed in Figures 3 and 4. The solid lines in these figures are the results of the theoretical analysis described below. Some information can be obtained by examining the general features of the spectra. The magnetic features almost disappear as the absorption width goes through a minimum at $T \approx 64$ K, indicating that the applied magnetic field is almost cancelled by the internal magnetic field in most directions. This implies that the internal field is opposite the applied field, as one expects for a contact-dominated internal field. The doublet–triplet structure of the 6 T, 195 K spectrum is similar to that of a diamagnet since $\langle \vec{S} \rangle$ and $\langle \vec{H}_{int} \rangle$ are small. The appearance of the triplet on the low-energy side indicates that the largest component of the electric field gradient (EFG) is positive and that the asymmetry parameter η is small. This would suggest that there is an excess of electron density in an oblate orbital of axial or near-axial symmetry.

Phenomenological Fits. The high-field variable-temperature data of [Fe(TPP)(OPh)]⁻ were initially analyzed by using the phenomenological model of the internal magnetic field.[7,9,28] This model is applicable when the observed paramagnetic hyperfine structure arises from the interaction between the nuclear spin and a single magnetic field. The nuclear hyperfine Hamiltonian in this approximation can be written as

$$\mathcal{H}_N = \mathcal{H}_q - g_n^* \beta_n \vec{H}_{app} \cdot (\vec{1} + \tilde{\omega}) \cdot \vec{I} \qquad (3)$$

The first term in eq 3 describes the quadrupole interaction

$$\mathcal{H}_q = \frac{eQV_{zz}}{4}\left[I_z^2 - \frac{5}{4} + \frac{\eta}{3}(I_x^2 - I_y^2) \right] \qquad \eta = \frac{V_{xx} - V_{yy}}{V_{zz}} \qquad (4)$$

where V_{zz} is the largest component of the EFG tensor. Q is the nuclear quadrupole moment. The second term in eq 3 is the Zeeman interaction between the nuclear spin and the effective field.

The term $\vec{H}_{app} \cdot \tilde{\omega}$ represents the internal field at the nucleus caused by the polarization of the electron magnetic moment; it

(21) Campbell, M. J. M. *Chem. Phys. Lett.* **1972**, *15*, 53.
(22) Larkworthy, L. F.; Fitzsimmons, B. W.; Patel, R. R. *J. Chem. Soc., Chem. Commun.* **1973**, 902.
(23) Zimmerman, R.; Spiering, H.; Ritter, G. *Chem. Phys.* **1974**, *4*, 133.
(24) Reiff, W. M. *Inorg. Chem.* **1974**, *13*, 239.
(25) Riley, D. P.; Merrell, P. H.; Stone, J. A.; Busch, D. H. *Inorg. Chem.* **1975**, *14*, 490.
(26) Fitzsimmons, B. W.; Al-Mukhtar, S. E.; Larkworthy, L. F.; Patel, R. R. *J. Chem. Soc., Dalton Trans.* **1975**, 1969.
(27) Lang, G.; Dale, B. W. *Nucl. Instrum. Methods* **1974**, *116*, 567.
(28) Kent, T. A.; Spartalian, K.; Lang, G.; Yonetani, T. *Biochim. Biophys. Acta* **1977**, *490*, 331.

is in general a function of both the temperature and applied field. At high temperatures the internal field should be simply proportional to the induced magnetic moment and the components of $\tilde{\omega}$ are expected to be field-independent and to vary as $1/T$ as in the Curie law limit of the susceptibility. At low temperatures, $\tilde{\omega}$ should be field-dependent if the model can be used at all.

The results shown in Figure 3 were produced by a least-squares minimization routine.[27] The initial fits assumed that the principal axis frames of EFG and $\tilde{\omega}$ coincided and were axially symmetric. Thus, the parameters $\omega_\perp$, ω_z, and Γ were varied in order to minimize the sum of the squares of the residuals between the theoretical and experimental spectra. These fits are shown as solid lines in Figure 3, and parameter values are listed in Table II. The uncertainty in the $\tilde{\omega}$ components is approximately ±0.02. The temperature dependence of $\omega_\perp$ and ω_z are displayed by using a log–log scale in Figure 5. The solid lines with slope −1 indicate a $1/T$ dependence.

This phenomenological model provided satisfactory fits only for the $T \geq 16$ K data in a field of 6 T. There are two major reasons this model failed for both the low-temperature and intermediate-field data. The first involves the electron spin relaxation rate. As the temperature is lowered, the relaxation rate decreases and the fast-relaxation assumption inherent in the phenomenological model is violated. This can be seen in the $T < 64$ K data, where the fits require a line width of up to twice the zero-field value. The second reason involves spin saturation. Consider a system in which a large magnetic field is applied to remove the degeneracy of the isolated spin multiplet. At very low temperatures only the ground state will be populated. The spin is saturated since it is insensitive to variations of the field strength and temperature. The phenomenon of spin saturation, which causes low-temperature deviation from the Curie law, is described by the Brillouin function in the quantum statistical formulation. Our phenomenological method is a linear theory and cannot reproduce the Mössbauer spectra in these saturation situations. This problem is evident in the 6 T data for $T \leq 32$ K, where the $\tilde{\omega}$ components deviate from the $1/T$ dependence, and in our complete failure to fit 6-T spectra for $T \leq 16$ K. Although our phenomenological fits are inferior to what follows below, they provide a parameterization of the data that is independent of electronic models and facilitate comparisons with other published data.

Spin-Hamiltonian Fits. In a more refined attempt to fit the Mössbauer spectra, we employ a $S = 2$ spin Hamiltonian[7,8,29-34] of the form

$$\mathcal{H} = \mathcal{H}_e + \mathcal{H}_{hf} \tag{5}$$

where $\mathcal{H}_e$ describes the purely electronic interactions or fine structure and $\mathcal{H}_{hf}$ describes the hyperfine interactions. In general, this Hamiltonian is of dimension $(2S + 1) \times (2I + 1)$, where S is the effective spin that describes the electronic state and I is the spin angular momentum of the nucleus. The orbital degeneracy can be ignored since we have a well-isolated spin multiplet of $2S + 1$ members. Our spin $\vec{S}$ is not the actual spin of the system but is closely related.

The electronic Hamiltonian is given by eq 1 and 2. The hyperfine Hamiltonian for the excited nuclear state can be written as

$$\mathcal{H}_{hf} = \mathcal{H}_q - g_n^* \beta_n \vec{H}_{app} \cdot \vec{I} + \vec{S} \cdot \tilde{A}^* \cdot \vec{I} \tag{6}$$

where $\tilde{A}^*$ is the magnetic hyperfine tensor, g_n^* is the nuclear gyromagnetic ratio, β_n is the nuclear magneton, and $+1/g_n^* \beta_n = -14.7$ T/(mm/s). The parameters with an asterisk refer to the excited nuclear state. The first term in eq 6 describes the quadrupole interaction, the second is the Zeeman interaction between the nucleus and an applied magnetic field, and the third term is the magnetic hyperfine interaction with the electrons.

We can reduce the dimensionality of the problem if we note that for applied magnetic fields greater than 1 mT the effect on the electrons of the magnetic field produced by the nucleus will be masked. In this situation the nuclear and electronic problems will be decoupled. Thus, we can calculate the Mössbauer spectra from eq 6 by replacing the electronic operators by their expectation values. We identify the quantity $-\langle \vec{S} \rangle \cdot \tilde{A}^* / g_n^* \beta_n$ as the internal magnetic field produced by the unpaired electrons so that the effective field seen by the nucleus is

$$\vec{H}_{eff} = \vec{H}_{app} - \langle \vec{S} \rangle \cdot \tilde{A}^* / g_n^* \beta_n \tag{7}$$

The magnetic hyperfine tensor $\tilde{A}^*$ usually has positive components in high-spin ferrous compounds, making $\tilde{A}^*/g_n^* \beta_n$ negative. The low-lying members of the spin multiplet have spin polarized opposite to the applied field so the internal field opposes the applied field. The nuclear ground state can be described by eq 6 and 7 except that $\mathcal{H}_q = 0$, $g_n = -1.749 g_n^*$, and $\tilde{A}/g_n = \tilde{A}^*/g_n^*$.

The electronic relaxation rate has a profound effect on the Mössbauer spectrum. In the slow relaxation limit, where the electron spin remains in a particular state for a long time, the Mössbauer spectrum is the result of an interaction between the nucleus and a magnetic hyperfine field produced by that particular state. For finite temperatures, each of the electronic states can be populated and each gives rise to its own Mössbauer spectrum. In practice, $\mathcal{H}_e$ is diagonalized and the spin expectation value is computed for each state. The spin expectation value is then used to compute a spectrum corresponding to that state. Individual spectra are then weighted by an appropriate Boltzmann factor and summed to produce the final Mössbauer spectrum. In contrast, in the fast relaxation limit the electron spin is assumed to relax rapidly among the available states during the lifetime of the excited iron nucleus. The Mössbauer spectrum in this case is the result of an interaction between the nucleus and a single magnetic field that is the thermal average of the fields associated with all the electronic states. In practice, $\mathcal{H}_e$ is diagonalized and the thermal average spin is computed. The Mössbauer spectrum is found by replacing $\langle \vec{S} \rangle$ in eq 6 by this thermal average. We have made no attempt in this paper to fit the Mössbauer spectra in the more complicated intermediate relaxation regime. High-field spectra recorded at 16–128 K and the $H \leq 3$ T spectra recorded at 4.2 K show evidence of intermediate relaxation.

Calculation of the low-temperature Mössbauer spectra for the coupled system involves a technical detail that we must now address. With $D = -1.6$ cm^{-1}, the low states on each iron site involve $S_z = \pm 2$. The combined states of two sites would be represented as $|+2, +2\rangle$, $|+2, -2\rangle$, $|-2, +2\rangle$, and $|-2, -2\rangle$. An applied field would raise the first, lower the last, and leave the middle pair unaffected and degenerate. This unsymmetric pair could as well be replaced by any pair of orthogonal linear combinations, including $|S\rangle$, $|A\rangle$, the symmetric and antisymmetric pair. In the slow relaxation regime the calculated Mössbauer spectrum would depend on which linear combination is assumed. This case is unlike the case of two coupled electrons[35] or the coupled ferric dimers,[9-13] for the exchange will not lift the present degeneracy and select the $|S\rangle$, $|A\rangle$ pair. We cannot tolerate a predicted spectrum that depends on details of the matrix diagonalization algorithm. We have elected to examine the two extremes. In method I we have made the electronic g factors of the iron sites differ by 0.01%. This guarantees that the unsymmetric states are chosen. These have nonzero internal field at a given iron nucleus. In a rough sense this artificial treatment may mimic the effect of the nuclear field upon the electron. In method II we have in addition inserted small off-diagonal terms Δ in the Hamiltonian matrix of eq 1. Δ has been adjusted to optimize the 4.2 K, 0.5-T spectrum. In zero field it would make the $|S\rangle$, $|A\rangle$

(29) Champion, P. M.; Lipscomb, J. D.; Munck, E.; Debrunner, P.; Gunsalus, I. C. *Biochemistry* **1975**, *14*, 4151.
(30) Schultz, C.; Debrunner, P. G. *J. Phys. (Les Ulis, Fr.)* **1976**, *36*, C6, 153.
(31) Zimmermann, R.; Huynh, B. H.; Munck, E.; Lipscomb, J. D. *J. Chem. Phys.* **1978**, *69*, 5463.
(32) Moura, I.; Huynh, B. H.; Hausinger, R. P.; Le Gall, J.; Xavier, A. V.; Munck, E. *J. Biol. Chem.* **1980**, *255*, 2493.
(33) Lang, G. *Q. Rev. Biophys.* **1970**, *3*, 1.
(34) Abragam, A.; Bleaney, B. *Electron Paramagnetic Resonance of Transition Ions*; Oxford University Press: London, 1970.
(35) Cohen-Tannoudji, C.; Diu, B.; Laloe, F. *Quantum Mechanics*; Wiley: New York, 1977; Vol. II, p 1003.

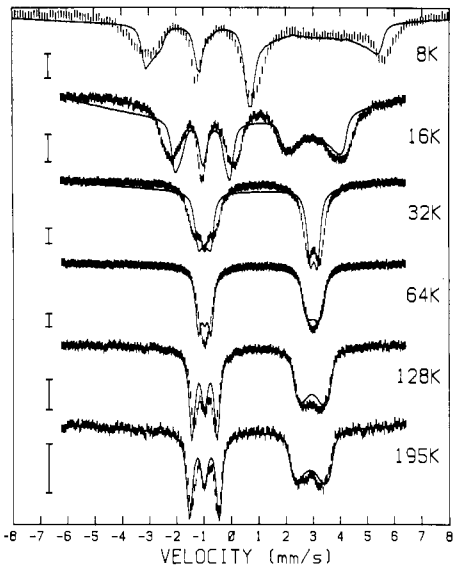

Figure 6. Mössbauer spectra of $[Fe(TPP)(OPh)]^-$ in a transverse magnetic field of 6 T at the temperatures indicated. The solid lines are based on spin Hamiltonian method I, using eq 1, 2, 5, and 6 with parameters listed in Table III except $\Delta = 0$. Method II results are indistinguishable from these. Vertical bars indicate 1% absorption.

Table III. $S = 2$ Spin-Hamiltonian Parameters for the Data in Figures 4 and 6[a]

T, K	ΔE_q, mm/s	Γ, mm/s	H_{app}, T	relax rate
4.2	4.008	0.25	6	slow
4.2	4.008	0.25	3	slow
4.2	4.008	0.25	1	slow
4.2	4.008	0.25	0.5	slow
8.0	4.003	0.25	6	fast
16.0	4.001	0.25	6	fast
32.0	3.994	0.25	6	fast
64.0	3.984	0.24	6	fast
128.0	3.946	0.24	6	fast
195.0	3.890	0.23	6	fast

[a] $D = -1.60$ (± 0.2) cm^{-1}, $E = 0$ (± 0.2) cm^{-1}, $J = -0.08$ (± 0.01) cm^{-1}, $\eta = 0$ (± 0.3), $V_{zz} > 0$, $\Delta g/g = 0.0001$, $\tilde{A}^*/g_n^*\beta_n$ = [−17.6 (± 1.0), −17.6 (± 1.0), −12.8 (± 1.0)] T/unit spin, and $\Delta = 0.0005$ cm^{-1} for all simulations.

pair eigenstates, with separation 2Δ. These states have zero internal field. It is possible that the actual antiferromagnetic interaction may lift the degeneracy in this way. Its traditional formulation as an exchange (last term of eq 1) is based largely on convenience and has a limited physical basis when ions with $S > {}^1/_2$ are involved.

The method I fits are shown as the solid lines in Figures 4 and 6 and are parameterized by the following values: $D = -1.60$ cm^{-1}, $E = 0$, $J = -0.08$ cm^{-1}, $\Delta g/g = 0.0001$, $\tilde{A}^*/g_n^*\beta_n$ = (−17.6, −17.6, −12.8) T/unit spin, $V_{zz} > 0$, and $\eta = 0$ with ΔE_q, Γ, and the relaxation rates listed in Table III. An estimation of the uncertainty in these values is given at the bottom of Table III. These fits assumed a common principal axis system for the EFG, the zero-field splittings, the electronic Zeeman interaction, and the magnetic hyperfine tensor. The slow-relaxation calculations were performed by considering only the 6 lowest of the 25 available electronic levels. This is a good approximation at low temperatures and high fields since only a few low-lying states are appreciably populated. At low fields this approximation is not as good. We justify its use by noting that the $J = 0$, $\Delta = 0$ dimer calculation using 6 out of 25 levels gives a very good approximation to the spectra predicted in an isolated-ion calculation using all 5 levels. Consideration of all 25 levels in a slow-relaxation dimer calculation is prohibited by computation expense. Fast-relaxation calculations were performed by considering all 25 electronic levels.

For comparison, the solid lines of Figure 7 are method II fits to the 4.2 K data recorded in various fields with the same parameters used in Figure 5 except that $\Delta = 0.0005$ cm^{-1}. The effect

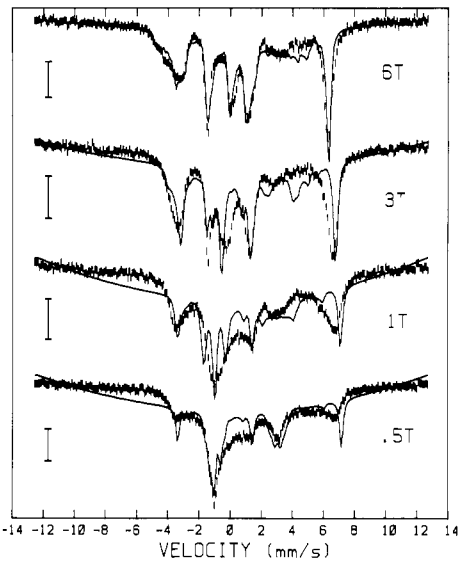

Figure 7. Mössbauer spectra of $[Fe(TPP)(OPh)]^-$ at 4.2 K and in transverse magnetic fields as indicated. The solid lines are based on spin Hamiltonian method II, using eq 1, 2, 5, and 6 with parameters listed in Table III. The curved base lines in the lower three simulations are artifacts of the fitting program, which in these poor-fit cases overestimates the counter solid angle effect. Vertical bars indicate 1% absorption.

of the Δ term can be most easily seen by comparing the 0.5-T spectra of Figures 4 and 7. In the absence of a magnetic field the Mössbauer spectrum consists of a quadrupole doublet with lines at approximately −1 and +3 mm/s. We see in Figure 7 that the method II calculation for the coupled case gives a line at +3 mm/s in agreement with the Mössbauer data. This line is the result of the nonmagnetic electronic level that is produced by the presumed degeneracy-lifting interaction between the spins of the dimer. In contrast, this line is absent in the method I spectra of Figure 4, so method II seems preferable. However, an alternative explanation for this feature might be the occurrence of fast spin relaxation for some crystal orientations. The effects of coupling on the Mössbauer spectra are small in general. They are also mixed, for the unwanted absorption at 4 mm/s in the 3-T calculations of Figures 4 and 7 is absent in an isolated-ion calculation. A sufficiently ingenious spin-coupling mechanism might give us the best of both schemes but is hardly appropriate. On the whole, we find that it is the combination of Mössbauer and susceptibility data that points to the spin coupling. In the 6-T field both of the coupled schemes give spectra that are indistinguishable from those of the uncoupled calculation.

The spin-Hamiltonian fits are generally acceptable and would probably be improved if we were able to include the effects of intermediate spin relaxation rates. While it is possible to vary D, E, J, and $\tilde{A}^*$ to optimize the fit of a particular spectrum, we have chosen common parameters to give reasonable fits to the data taken as a whole.

Discussion

In order to understand the electronic structure of $[Fe(TPP)(OPh)]^-$, we examine the sources of the internal magnetic field. The internal field produced by the $(3d)^6$ electronic configuration can be written as

$$\vec{H}_{int} = -P/g_n^*\beta_n \sum_{j=1}^{6} [\langle \vec{l}_j \rangle + \langle 3(\hat{r}_j \vec{s}_j)\hat{r}_j - \vec{s}_j \rangle - \kappa \langle \vec{s}_j \rangle] \quad (8)$$

where P and κ are constants. The terms in brackets are the orbital, dipole, and Fermi contact contributions, respectively. The constants $P/g_n^*\beta_n = 61.6$ T and $\kappa = 0.35$ were determined by Lang and Marshall[36] by fitting high- and low-spin ferric hemoglobins. While these values may require modification in the present ferrous

(36) Lang, G.; Marshall, W. *Proc. Phys. Soc., London* **1966**, *87*, 3.

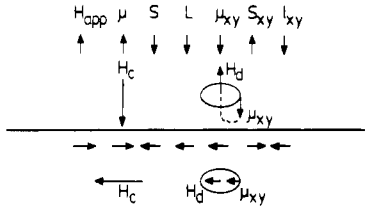

Figure 8. Directions of the various terms of eq 8 for the applied magnetic field in both the axial and transverse directions.

case, we will assume them for the discussion that follows.

The high-spin ferrous d electrons may be described as a full subshell of parallel-spin electrons plus an extra electron with opposite spin. Orbital and dipolar contributions of the subshell vanish; these contributions are provided by the extra electron only. It is convenient to consider eq 8 for the lowest electronic state in the presence of a very strong applied magnetic field that defines the positive direction. In this deep saturation condition the electronic moment will lie along H_{app}, and the net spin $\vec{S}$ will point in the negative direction. The Fermi contact term involves all electrons and depends on the total spin of magnitude 2. Equation 8 then gives the contact interaction as $H_{contact} = P\kappa/g_n^*\beta_n(-2) = -43.1$ T. If the extra electron is in an $|xy\rangle$ orbital, then the dipolar contribution to the internal field is axially symmetric and has a value of $H_{dipole,z} = P\kappa/g_n^*\beta_n(^4/_7)(^1/_2) = 17.6$ T in the axial direction and $H_{dipole,\perp} = -P\kappa/g_n^*\beta_n(^2/_7)(^1/_2) = -8.8$ T in the transverse direction. The orbital motions of the 3d electrons under consideration should give a positive contribution to the internal field in eq 8 since the spin–orbit interaction favors parallel $\vec{L}$ and $\vec{S}$ in shells that are more than half-filled. The orbital contribution is generally small in a coordinated complex as compared with that in the free ion since bonding interactions with the ligands tend to localize the valence electrons in space and quench their orbital angular momentum. We have some indication that this condition is true for the present case since the small temperature dependence of the quadrupole splitting is suggestive of a well-isolated orbital ground state and the high-temperature N_{eff} value is only a few percent higher than the spin-only value. Thus, if the extra electron is in the oblate $|xy\rangle$ orbital, we expect that the saturation value of the internal field will have a smaller magnitude in the axial direction, with $H_{int,z}/H_{int,\perp} = (-43.1 + 17.6)/(-43.1 - 8.8) = 0.49$. Figure 8 shows schematically the directions of relevant quantities and indicates how the dipolar sign is determined. If the extra electron is in a $|3z^2 - r^2\rangle$ prolate orbital, the dipolar contributions would have signs opposite to the above, and $H_{int,z}/H_{int,\perp} = (-43.1 - 17.6)/(-43.1 + 8.8) = 1.8$.

While we do not achieve complete spin saturation in our measurements, our $\tilde{A}^*$ tensor does predict this saturation internal field, since $\vec{H}_{int} = -\langle\vec{S}\rangle\cdot\tilde{A}^*/g_n^*\beta_n$. The saturation condition corresponds to $\langle S\rangle$ having component -2 along H_{app}, so the predicted saturation fields are $(-35.2, -35.2, -25.6)$ T, with the ratio $H_{int,z}/H_{int,\perp} = 0.73$.

At high temperature we expect the induced electron magnetic moment to become relatively direction-insensitive, and under these conditions the ratio of ω components should be the ratio of saturation fields. We see from Table II that the high-temperature ω ratio is about 0.75. Thus, the magnetic hyperfine interactions clearly indicate that the extra electron in the present case is in a fairly well isolated $|xy\rangle$ orbital. This conclusion is consistent with the positive sign and small temperature dependence of the quadrupole splitting.

The electronic structure of $[Fe(TPP)(OPh)]^-$ appears to be similar to that of the P-460 center of the protein hydroxylamine oxidoreductase.[1] The quadrupole splittings are quite close (+4.018 mm/s for the model and +4.21 mm/s for the protein at 4.2 K), and both share an axial EFG with $V_{zz} > 0$. While a detailed determination of the magnetic properties of the protein was not made, we note that the estimated direction-averaged magnetic hyperfine tensor was found to be $\tilde{A}^*(av)/g_n^*\beta_n = -15.9$ T/unit spin for the protein while we found -16.0 T/unit spin for $[Fe(TPP)(OPh)]^-$.

Table IV. $S = 2$ Spin-Hamiltonian Parameters for Reduced Protocatechuate 3,4-Dioxygenase,[31] Reduced Desulforedoxin,[32] and $[Fe(TPP)(OPh)]^-$

	3,4-Pcase	DX	$[Fe(TPP)(OPh)]^-$
D, cm^{-1}	−6	−6	1.60
E/D	0.25	0.19	0[d]
J, cm^{-1}	0[d]	0[d]	−0.08
g_x	2.09[c]	2.08[c]	2[d]
g_y	2.02[c]	2.02[c]	2[d]
g_z	2.20[c]	2.20[c]	2[d]
$A_x^*/g_n^*\beta_n$, T/unit spin	−25.0	−20.0	−17.6
$A_y^*/g_n^*\beta_n$, T/unit spin	−24.0	−20.0	−17.6
$A_z^*/g_n^*\beta_n$, T/unit spin	−11.0	−6.7	−12.8
η	0.25	0.35	0[d]
ΔE_q, mm/s[b]	+3.13	+3.35	+4.01
δ, mm/s[a]	+1.21	+0.70	+1.03
β, deg[e]	27	10	0[d]

[a] Values at 4.2 K relative to metallic iron at room temperature. [b] Values at 4.2 K. [c] Determined by perturbation expressions and methods of ref 23 and 32. [d] Not a variable of the calculation. [e] β is the polar angle between the z axis of the principal axis frames of the $\tilde{g}$ tensor and the EFG. The zero-field splittings and the $\tilde{g}$ tensor share a common principal axis frame in these calculations.

Information about the magnetic properties of the several synthetic compounds that are probably similar to $[Fe(TPP)(OPh)]^-$ has not been given.[2-5] Fortunately there are several reported investigations of biological high-spin ferrous compounds with oblate ground states in which more extensive magnetic information is available.[31,32] We restrict our comparisons to compounds having negative values of the zero-field splitting parameter D since we found it impossible to reconcile the Mössbauer data of $[Fe(TPP)(OPh)]^-$ for $D > 0$. The results of these comparisons are displayed in Table IV.

The first study, on reduced protocatechuate 3,4-dioxygenase (3,4-Pcase), by Zimmermann[31] is suggestive of a low-symmetry environment for the ferrous ion. This fact is reflected by the nonzero Euler angle β that relates the principal axis frame of the electronic parameters (D, E, and g) to the principal axis frame of the EFG. Aside from symmetry arguments, a similarity between 3,4-Pcase and the present compound is that the weak temperature dependence of the magnitude of the quadrupole splitting indicates a well-isolated orbital ground state in both cases. The spin-Hamiltonian formalism is generally not applicable to systems where the orbital ground state is not well isolated, so the temperature dependence of the quadrupole splitting provides a reliable indication of applicability. The results of Moura[32] on reduced desulforedoxin (DX) are similar to that of 3,4-Pcase except that the rotation of the zero-field splitting coordinate axis with respect to those of the EFG is less pronounced.

We see from Table IV that the saturation internal fields of these compounds are quite similar. If we ignore the slight deviation from axial symmetry for the 3,4-Pcase compound, all compounds have $A_\perp^*/g_n^*\beta_n$ and $A_z^*/g_n^*\beta_n$ negative with $|A_z^*/g_n^*\beta_n|/|A_\perp^*/g_n^*\beta_n| < 1$. This is consistent with an oblate ground state and a contact-dominated internal field modified by a dipole term due to the extra electron. A prolate ground state would require $|A_z^*/g_n^*\beta_n|/|A_\perp^*/g_n^*\beta_n| > 1$. These compounds also share $D < 0$. A crystal field calculation gives $D > 0$ for low $|xy\rangle$ and large cubic field, but $D < 0$ requires $|x^2 - y^2\rangle$ to intrude and mix with the ground state through the spin–orbit interaction.

The deduction of oblate ($|xy\rangle$) character for the sixth d electron identifies the ground state as $^5A_2$ in C_{2v} symmetry or $^5B_2$ in C_{4v} symmetry. The magnetic evidence is in our view the most convincing since only the unpaired valence electrons contribute. EFG evidence is always complicated by the possibility of significant contributions from the lattice or, more likely, from bonding orbitals. Since all of our measurements have been performed on powder samples, we have not determined the orientation of our assumed coordinate system within the molecule. We note that our measurements imply axial symmetry. The simplest and most likely assumption is that z is along the heme normal, and the

oxygen anion raises the energy of the $\{|xz\rangle, |yz\rangle\}$ pair relative to that of $|xy\rangle$. The 4-fold symmetry is reduced to 2-fold by the phenol ring, but the rhombic crystal field splitting apparently is small.

We note that the magnitude of quadrupole splitting in [Fe(TPP)(OPh)]$^-$ and the other hemes with positive EFG is much larger than that of the deoxyhemes (typically 2.2 mm/s). Both magnetic and quadrupole interactions suggest that the latter have prolate ground states.[7,8,28,37] Interpretations[28] of single-crystal measurements[38] are consistent with this being a $|3z^2 - r^2\rangle$ orbital along a z axis that is roughly in the (1, 1, 1) direction relative to the usual heme coordinate system. The larger temperature dependence of ΔE_q on the deoxyhemes suggests the possibility that the orbital splittings are small and that this permits considerable spin–orbit mixing and consequent reduction of the low-temperature quadrupole splitting. We believe that this reduction is a minor effect at best, since the orbital mixing required for a significant reduction would result in a much larger zero-field-splitting D value and a much greater orbital moment than the susceptibility measurements[39-41] imply. The most detailed published fitting[42] of the deoxyheme quadrupole splitting and its temperature dependence has a large number of adjustable parameters. It yields the wrong sign for the quadrupole interaction, and its implications for magnetic properties have not been worked out.

It is likely that lattice or bonding orbital contributions are important in making the positive quadrupole splittings large. We note that high-spin and intermediate-spin ferric hemes all have positive quadrupole interactions, with splittings of the former ranging up to 1.1 mm/s and the latter up to 3.6 mm/s.[43,44] (The oxygen-bridged dimers are exceptions.[43]) It is generally assumed that all these ferric cases represent mixtures of ^{6}A and ^{4}A in various proportions.[45] Neither the pure states nor their mixtures have charge asymmetry capable of producing a quadrupole interaction, so other sources are implied. We note that large ^{4}A admixture implies a high-energy antibonding $|x^2 - y^2\rangle$ orbital and hence a strong mixing of $|x^2 - y^2\rangle$ with the in-plane ligand orbitals. The trend to large ΔE_q as $g_\perp$ approaches 4 is thus seen as the result of increasing $|x^2 - y^2\rangle$ character in the bonding orbital.[13] The high-spin alkoxoiron(III) compound Fe(TPP)(OMe) with $\Delta E_q \approx +0.8$ mm/s may provide the most relevant comparison with the present case.[43,46] In a rough approximation we may regard it as having the same nonvalence contribution to the quadrupole interaction as [Fe(TPP)(OPh)]$^-$. Its $|x^2 - y^2\rangle$ bonding charge would directly add to the quadrupole field of our presumed $|xy\rangle$ valence electron. $S = 1$ ferrous tetraphenylporphyrin[47] is a ferrous heme in which the magnetic features of the Mössbauer spectra have been successfully related to a simple electronic model. In this and in the closely related case of ferrous phthalocyanine[48] it is necessary to postulate a large in-plane electronic charge from lattice or bonding electron contributions, i.e., a large nonvalence contribution to the quadrupole interaction that is positive and is aligned at least roughly with the heme normal. In a similar way there is a strong tendency for the low-spin ferrous hemes, which have no valence contribution, to have positive EFG. Thus, in the preponderance of ferric and ferrous cases that have been treated in some detail and seem relatively clear-cut, there appears to be an excess of nonvalence electronic charge in the heme plane. While this would augment the quadrupole field of the presumed $|xy\rangle$ ground orbital of [Fe(TPP)(OPh)]$^-$ and similar compounds, it would also reduce the net quadrupole field of the prolate ground-state orbital of the trigonally distorted deoxyhemes. Incidentally, this mechanism may also provide an explanation for the fact that the magnetic properties of the deoxyhemes appear to have axial symmetry while the EFG has a fairly high asymmetry parameter.

In conclusion, we feel that an analysis of the paramagnetic behavior by the techniques of magnetic susceptibility and Mössbauer spectroscopy has led to some insight into the electronic structure of the synthetic high-spin ferrous compound [Fe(TPP)(OPh)]$^-$. We hope that this and similar efforts will eventually permit a good understanding of the nature of ferrous hemes in general.

Acknowledgment. This work has been carried out at The Pennsylvania State University under National Institutes of Health Grant HL-16860. Work at the University of Southern California has been carried out under National Institutes of Health Grant GM-23851.

Registry No. [Na(dibenzo-18-crown-6)(THF)$_2$][Fe(TPP)(OPh)], 117678-67-8; Fe(TPP)(THF)$_2$, 29189-60-4; hydroxylamine oxidoreductase, 9075-43-8.

(37) Kent, T. A.; Spartalian, K.; Lang, G. *J. Chem. Phys.* **1979**, *71*, 4899.
(38) Maeda, Y.; Harami, T.; Trautwein, A.; Gonser, U. *Z. Naturforsch.* **1976**, *31B*, 487.
(39) Nakano, N.; Otsuka, J.; Tasaki, A. *Biochim. Biophys. Acta* **1971**, *236*, 222.
(40) Alpert, A.; Banerjee, R. *Biochim. Biophys. Acta* **1975**, *405*, 114.
(41) Nakano, N.; Otsuka, J.; Tasaki, A. *Biochim. Biophys. Acta* **1972**, *278*, 355.
(42) Eicher, H.; Bade, D.; Parak, F. *J. Chem. Phys.* **1976**, *64*, 1446.
(43) Sams, J. R.; Tsin, T. B. *The Porphyrins*; Dolphin, D., Ed.; Academic: New York, 1979; Vol. 4, Chapter 9.
(44) Spartalian, K.; Lang, G.; Reed, C. A. *J. Chem. Phys.* **1979**, *71*, 1823.
(45) Maltempo, M. M.; Moss, T. H. *Q. Rev. Biophys.* **1976**, *9*, 181.
(46) Kobayashi, H.; Maeda, Y.; Yanagawa, Y. *Bull. Chem. Soc. Jpn.* **1970**, *43*, 2342.
(47) Lang, G.; Spartalian, K.; Reed, C. A.; Collman, J. P. *J. Chem. Phys.* **1978**, *69*, 5424.
(48) Dale, B. W. *Mol. Phys.* **1974**, *28*, 503.